

Aeolian sand ripples: experimental evidence of coarsening and saturation.

Bruno Andreotti and Philippe Claudin

*Laboratoire de Physique et Mécanique des Milieux Hétérogènes (UMR CNRS 7636),
ESPCI, 10 rue Vauquelin 75231 Paris Cedex 05, France.*

Olivier Pouliquen

IUSTI, Université de Provence – CNRS, 5 rue Enrico Fermi, 13453 Marseille Cedex 13, France.

(Dated: December 13, 2018)

We report an experimental investigation of aeolian sand ripples, performed both in a wind tunnel and on stoss slopes of dunes. Starting from a flat bed, we can identify three regimes: appearance of an initial wavelength, coarsening of the pattern and finally saturation of the ripples. We show that both initial and final wavelengths, as well as the propagative speed of the ripples, are linear functions of the wind velocity. Investigating the evolution of an initially corrugated bed, we exhibit non-linear stable solutions for a finite range of wavelengths, which demonstrates the existence of a saturation in amplitude. These results contradict most of the models, which all predict a constant initial length of destabilization as well as a perpetually increasing wavelength.

PACS numbers: 45.70.-n, 47.54.+r, 05.45.-a

The surface of aeolian sand dunes is not smooth but is usually formed into regular patterns of ripples, transverse to the wind [1]. Their wavelength ranges from the centimeter to the meter with a constant aspect ratio ($\simeq 4\%$) [2]. Although many different models have been proposed to explain the formation and evolution of aeolian ripples [3, 4, 5, 6, 7, 8, 9, 10], very few field observations [1, 2, 11] and controlled experiments [12] have been performed so far. By contrast with dunes or subaqueous ripples which result from a hydrodynamic instability induced by the interaction between shape and flow [1], aeolian ripples are of different nature and result from a screening instability [3]. When the ‘saltoms’ – high energy grains – collide the sand bed, they eject grains of smaller energy, ‘reptons’. The windward slope of a small bump is submitted to more impacts than the lee slope, so that the flux of reptons, which is higher uphill than downhill, makes the bump amplify.

Most of the models agree for the linear stage of the instability – see [4] for a pedagogical review. They assume that the reptons remain trapped by the bed after a single hop of length a , distributed according to a distribution $P(a)$. The saltoms are only considered as an external reservoir which brings energy into the system. On this basis, the most unstable wavelength λ_0 is found to scale on the reptation length $\bar{a} = \int da a P(a)$. Besides, the most recent investigations of sand transport, both experimental [13, 14] and theoretical [15, 16], indicate that $P(a)$ is independent of the wind shear velocity u^* , which implies that \bar{a} scales on the grain diameter d . The initial wavelength of the ripples λ_0 is thus expected to be independent of the wind strength. In the non-linear regime, aeolian ripples have been one of the most extensively studied systems presenting coarsening. Two scenarios are evoked. The wavelength can increase by a phase instability (negative diffusion) leading to a

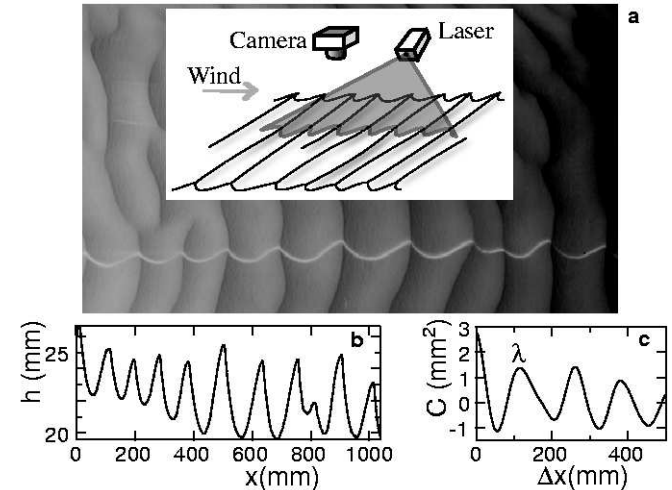


FIG. 1: **a** Experimental set up and measurement method. Picture of the sand ripples obtained for $u^* = 1.4 u_{th}$. The red line is the laser trace. **b** Profile $h(x)$ from the laser line. **c** Autocorrelation of the profile. The position first peak gives the mean wavelength. The value at zero gives the amplitude.

continuous stretching of the pattern [17]. Alternatively, ripples may be considered as locally interacting objects that undergo successive merging [12, 18]. In both cases, one predicts a perpetual increase of $\lambda(t)$ as the logarithm of time or as a power law of small exponent. However, common field observations clearly evidence steady patterns driven by a wind permanently blowing for hours. To the best of our knowledge, only one recent model predicts a saturation of ripples wavelength at long time [6]. Is the apparent saturation of λ in the field due to the inherent variability of the wind conditions? Is it observed under controlled conditions? How far can we trust the usual prediction of linear stability analysis? This study

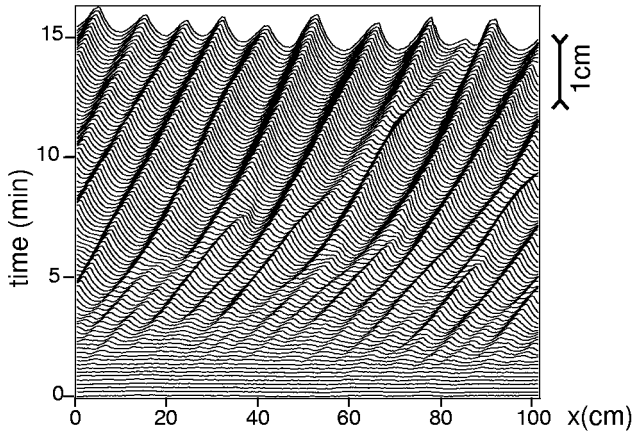


FIG. 2: Spatio temporal diagram for $u^* = 1.4 u_{th}$.

is an attempt to answer these questions.

Experimental set-up – We have performed experiments both in a wind tunnel (1 m wide, 0.5 m high and 4.5 m long) and in the barchan field extending between Tarfaya and Laayoune in Morocco. In the wind tunnel, the wind is precisely controlled and can reach $u^* \sim 0.7$ m/s but the sand flux is not fully saturated due to the limited length of the sand bed (3 m). In the field, the sand supply is almost unlimited and the flux is saturated but the wind strength fluctuates. In both situations, the sand grains – Hostun sand in the lab and quartz/lime mixture in the field – are $180 \mu\text{m}$ in diameter and the measured shear velocity threshold for saltation is $u_{th} \sim 0.22$ m/s. To measure the surface deformation, a laser sheet is inclined at some low angle to the bed (Fig. 1). Pictures are taken from above using a 2240×1680 digital camera. The profile $h(x, t)$ is detected by a correlation method which insures a precision of $40 \mu\text{m}$. The patterns obtained are usually quasi-periodic and can be characterized by an average wavelength λ and an amplitude A . As the number of wavelengths is small, we measure λ as the first maximum of the autocorrelation function $C(\Delta x, t) = \langle h(x, t)h(x + \Delta x, t) \rangle - \langle h(x, t) \rangle^2$ computed over the full picture (Fig. 1c). The amplitude is defined from the rms value of h : $A(t) = 2\sqrt{2C(0, t)}$.

Instability of a flat bed – We first study the time evolution of an initially flat bed. The spatio-temporal diagram of a typical such experiment is displayed in Fig. 2 and the corresponding time evolution of amplitude and wavelength in Fig. 3. Identifying a linear regime is not an easy task. A gentle linear instability – with a growth rate presenting a narrow peak in λ – is usually characterised by an exponential growth of the amplitude and a plateau in wavelength. Here, tiny structures with a small wavelength show up after a short time (~ 1 min for this run). Their growth in amplitude is consistent with an exponential when A is smaller than, say, 1 mm

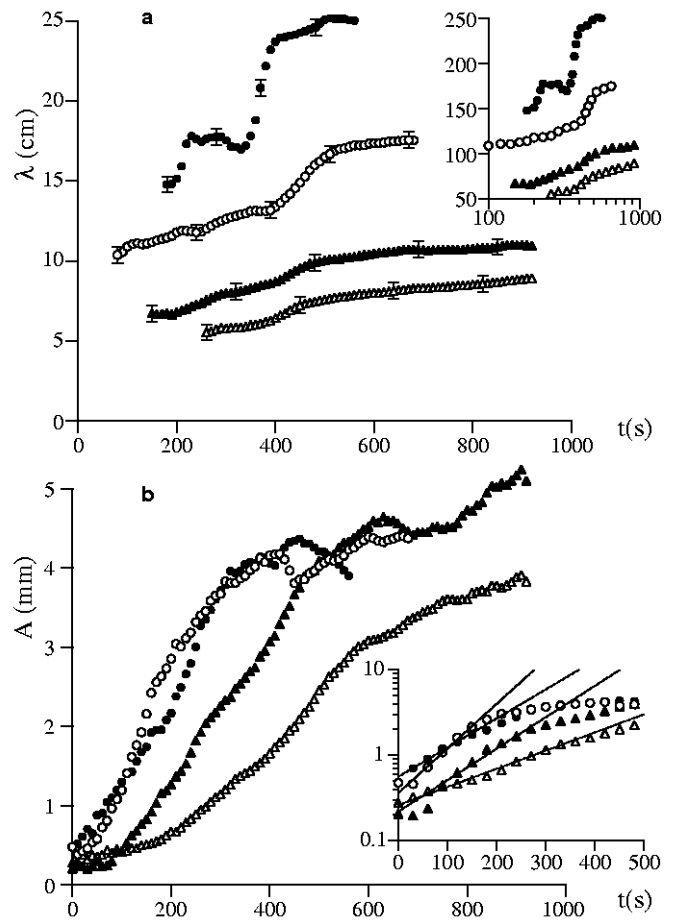


FIG. 3: Time evolution from a flat bed for different values of the shear velocity: $u^* = 1.3 u_{th}$ (\triangle), $u^* = 1.4 u_{th}$ (\blacktriangle), $u^* = 1.8 u_{th}$ (\circ), $u^* = 2.3 u_{th}$ (\bullet). **a** Wavelength $\lambda(t)$. **b** Amplitude $A(t)$. Inserts: horizontal or vertical log scales.

i.e. 6 grain sizes. However, a peak clearly appears in the autocorrelation function $C(\Delta x, t)$ only close to the end of this period. This tiny plateau still allows to define the initial wavelength λ_0 . As soon as they are visible, the ripples start merging so that the pattern exhibits coarsening. The increase of amplitude and wavelength progressively slows down and after some time (typically ~ 10 min), the pattern tends to ‘saturate’: the ripples essentially propagate without changing shape and amplitude anymore. We take λ_∞ as the average of λ over the last two minutes. As emphasised by the log scale in time, this ultimate regime could also be interpreted as a slow drift in λ [12]. Settling this issue would require at least one more decade in time (few hours), which is difficult to achieve in our wind tunnel due to the global erosion of the bed (a sand layer few centimetres thick disappears after typically half an hour) and to the convective nature of the instability (the entrance conditions can influence the measurement zone).

Evolution of an initially corrugated bed – To bypass the

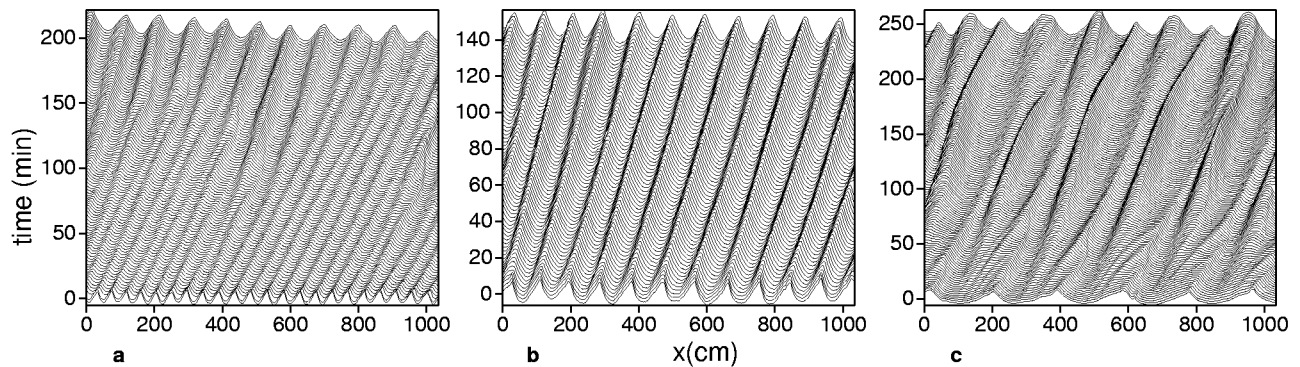


FIG. 4: Spatio-temporal evolution in the wind-tunnel of an initially corrugated bed for $u^* = 1.3 u_{th}$ and for different initial wavelengths: **a** $\lambda = 5$ cm; **b** $\lambda = 9.3$ cm; **c** $\lambda = 13.5$ cm.

problem, we have performed experiments in which we do not start from a flat bed but from a corrugated surface. A periodic ripple profile is initially engraved with a card-board pattern on the bed and is then let free to evolve. The influence of initial wavelength and amplitude is systematically explored, the shape remaining that of a developed ripple. The first result concerns the case when the engraved pattern has the same wavelength λ_∞ and same amplitude A_∞ as measured in 'natural conditions', i.e. starting from a flat bed. The ripples do not evolve at all and the pattern purely propagates (Fig. 4b), showing that a saturated state exists. If we start from the same λ but with a larger or a smaller amplitude, the pattern

converges back to the same shape (A_∞, λ_∞) by adjusting its amplitude. If we start from the same A but a slightly different λ , the patterns keeps this new wavelength and selects a new amplitude (Fig. 5). We can thus conclude that, depending on the initial conditions, the pattern converges toward different stable non-linear solutions. The saturated state observed starting from a flat bed is one solution among the finite band of wavelengths for which stable ripple patterns can be observed. If we start from a too large λ , the pattern destabilizes by changing its wavelength, forming substructures on the windward slope (generation of harmonics) as shown in Fig. 4c. Too small wavelengths are also unstable as the pattern coarsens due to merging (period doubling) (Fig. 4a). In the (A, λ) diagram representing the different initial conditions (Fig. 5), one can then determine a stable region where the engraved pattern does not change wavelength, an unstable region leading to coarsening for $\lambda \lesssim 60$ mm and an unstable region leading to a windward slope instability. These observations hold in the wind tunnel as well as for our field experiments (not shown).

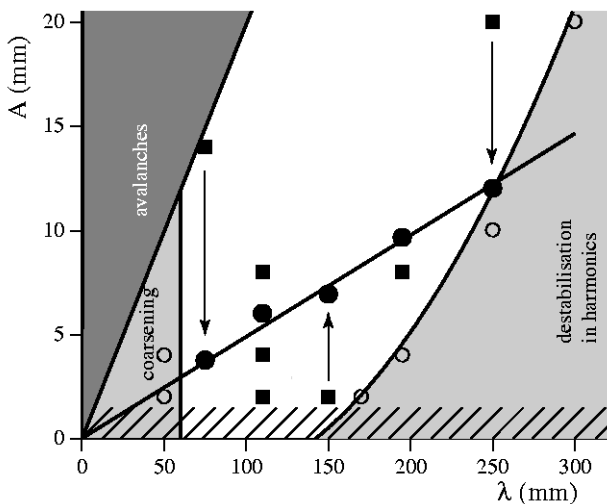


FIG. 5: Stability diagram of ripples of initial wavelength λ and amplitude A for $u^* = 1.3 u_{th}$. Outside the locking zone (\circ), the pattern destabilizes by generation of harmonics (right) or sub-harmonics (left). Starting in the central region (\blacksquare), λ stays constant and A readapts to reach a stable steady solution (\bullet). Very large amplitudes cannot be imposed as avalanche processes take place. Hatched region is beyond experimental access.

Parametric study – Once we have shown that the final pattern observed starting from a flat bed corresponds to a saturated state, we can systematically study the influence of the wind on the natural ripples characteristics. Fig. 6a shows the selection of the aspect ratio for different wind strengths. While the aspect ratio remains constant in the field ($A \sim 0.04\lambda$), the amplitude saturates in the wind tunnel at large u^* . This discrepancy may be related to the unsaturated state of the sand flux. The initial and final wavelengths are plotted as a function of the wind speed in panel b. By contrast with standard predictions, they both increase linearly with u^* . Interestingly, the initial wavelength λ_0 vanishes at the transport threshold and $\lambda_\infty(u^*)$ is almost parallel. The same tendency holds for field measurements, although scattering is observed due to wind fluctuations. In a similar way, the phase velocity c_∞ of saturated ripples increases linearly with $u^* - u_{th}$ (Fig. 6c). The influence of the sand to air

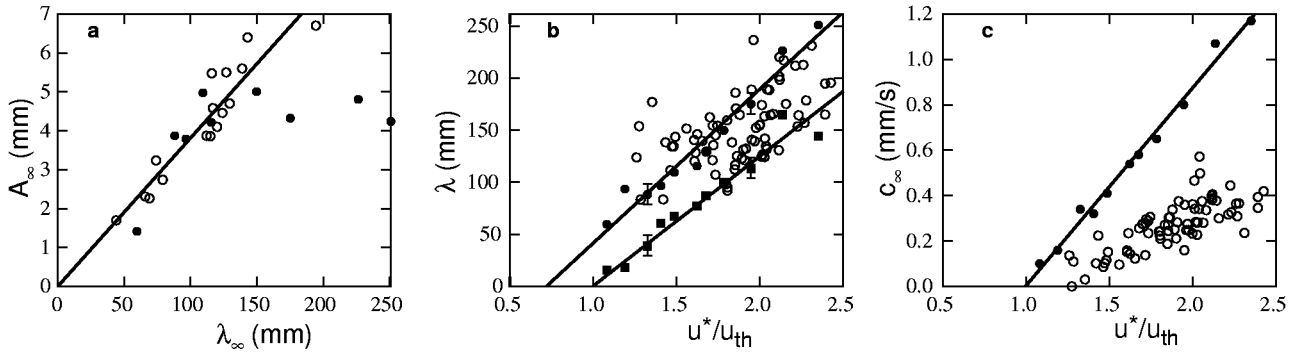


FIG. 6: **a** A as a function of λ for different wind velocities in the wind tunnel (●) and in the field (○). **b** Initial (■) and final (●) wavelength (wind tunnel data) as a function of the imposed flow velocity u^* . For field data (○), the wavelength – assumed saturated – is plotted as a function of the wind speed averaged over few minutes. **c** Propagation velocity of developed ripples as a function of the wind speed for free evolving ripples in the wind tunnel (●) and in the field (○). c_∞ is about three times smaller in the field, perhaps due to the larger wind fluctuations.

density ratio ρ_{sand}/ρ_{air} has not been tested experimentally. However, the inertial length $\rho_{sand}/\rho_{air} d$ is a key quantity for aeolian transport [16], which suggests the following scalings:

$$\lambda_0 = 0.27 \frac{\rho_{sand}}{\rho_{air}} \left(\frac{u^*}{u_{th}} - 1 \right) d, \quad (1)$$

$$c_\infty = 2.2 \frac{\rho_{air}}{\rho_{sand}} \left(\frac{u^*}{u_{th}} - 1 \right) \sqrt{gd}, \quad (2)$$

with a numerical prefactor determined from the data. Furthermore, this scaling would give an explanation for the decametric wavelengths of Martian ripples, formed in an atmosphere 80 times lighter [19].

Conclusion – Two main conclusions can be drawn from this study. First, the linear dependence of the most unstable wavelength with the wind speed rules out our theoretical understanding of ripples formation and sand transport in general. As λ_0 turns out to be much larger than the value predicted by Anderson-like models ($6\bar{a} \sim 60d \sim 10$ mm), there should exist a yet unknown mechanism stabilizing small wavelengths. Second, we have shown the existence of a whole family of stable non linear solutions. Future models should then be able to recover the band of wavelengths for which ripple patterns are stable, as well as the saturation of λ when starting from a flat bed.

In this work, we have studied the one dimensional dynamics of the ripples along the wind direction. However, a complex dynamics exists in the transverse direction too and the formation of defects is known to play a significant role in coarsening processes and in the route towards regular pattern [12, 18]. It then suggests to investigate the density of defects to characterize the degree of saturation of the pattern. Finally, ripples could be of practical interest for field experimentalist as a non intrusive measurement of the reptation sand flux. From mass conservation,

one expects the reptation flux to scale as the product of λ by c . The scalings (1) and (2) are indeed compatible with $q_{rep} \propto \frac{\rho_{air}}{\rho_{sand}} (u^* - u_{th}) \sqrt{\frac{d}{g}}$, as predicted in a recent model [16] – note that $\rho_{air} u_{th}^2 \propto \rho_{sand} g d$. More work is necessary to confirm this idea.

We wish to thank Florence Naaim and the ETNA group of the Cemagref (Grenoble) for the use of their wind tunnel and for their kind help during the experiments. This study was supported by the french ministry of research through an ‘ACI Jeunes C’.

- [1] R.E. Bagnold, *The physics of blown sand and desert dunes*, Chapman and Hall, Methuen, London (1941).
- [2] J.M. Ellwood, P.D. Evans and I.G. Wilson, *J. Sed. Petrology* **45**, 554 (1975).
- [3] R. Anderson, *Sedimentology* **34**, 943 (1987).
- [4] Z. Csahók *et al.*, *Eur. Phys. J. E* **3**, 71 (2000).
- [5] L. Prigozhin, *Phys. Rev. E* **60**, 729 (1999).
- [6] H. Yizhaq, N.J. Balmforth and A. Provenzale, *Physica D* **195**, 207 (2004).
- [7] R.B. Hoyle and A. Mehta, *Phys. Rev. Lett.* **83**, 5170 (1999).
- [8] D.A. Kurtze, J.A. Both and D.C. Hong, *Phys. Rev. E* **61**, 6750 (2000).
- [9] O. Terzidis, P. Claudin and J.-P. Bouchaud, *Eur. Phys. J. B* **5**, 245 (1998).
- [10] H. Nishimori and N. Ouchi, *Phys. Rev. Lett.* **71**, 197 (1993).
- [11] R.P. Sharp, *J. Geology* **71**, 617 (1963).
- [12] B.T. Werner and D.T. Gillespie, *Phys. Rev. Lett.* **71**, 3230 (1993).
- [13] J.D. Iversen and K.R. Rasmussen, *Sedimentology* **46**, 723 (1999).
- [14] F. Rioual, A. Valance and D. Bideau, *Phys. Rev. E* **62**, 2450 (2000).
- [15] R.S. Anderson and P.K. Haff, *Science* **241**, 820 (1988).
- [16] B. Andreotti, *J. Fluid Mech.* **510**, 47 (2004).

- [17] P. Politi and C. Misbah, Phys. Rev. Lett. **92**, 090601 (2004).
- [18] K.H. Andersen *et al.*, Phys. Rev. Lett. **88**, 234302 (2002).
- [19] www.markcarey.com/mars/mars-rover-photos.html.